Rare Metal Materials and Engineering
Volume 55, Issue 6, June 2026
Available online at www.rmme.ac.cn

Science Press

Cite this article as: Zhao Yunxing, Wang Di, Ma Dexin, et al. Effect of Dendrite Refinement on Microstructure and Stress Rupture Properties of Third-Generation Nickel-Based Single-Crystal Superalloys[J]. Rare Metal Materials and Engineering, 2026, 55(06): 1393-1399. DOI: https://doi.org/10.12442/j.issn.1002-185X.20250275.

ARTICLE

Effect of Dendrite Refinement on Microstructure and Stress Rupture Properties of Third-Generation Nickel-Based Single-Crystal Superalloys

Zhao Yunxing[2,3], Wang Di[1,2], Ma Dexin[2,3], Wei Jianhui[2,3], Cheng Bowen[3], Sun Hongyuan[2,3], Xu Weitai[3], Huang Zaiwang[1,2]

[1] State Key Laboratory of Powder Metallurgy, Central South University, Changsha 410083, China; [2] Powder Metallurgy Research Institute, Central South University, Changsha 410083, China; [3] Shenzhen Wedge Aviation Technology Co., Ltd, Shenzhen 518045, China

Abstract: A third-generation single-crystal superalloy WZ30 was used to prepare single-crystal samples with varying dendrite spacings under different processing techniques. The microstructure and stress rupture properties were studied and compared. The results show that, by improving the thermal-insulation effect between heating zone and cooling zone of the directional solidification furnace, the average primary dendrite spacing of the as-cast sample is reduced from 415 μm to 251 μm, leading to a noticeable refinement of dendrite and eutectic structure. At the same time, dendrite refinement can simultaneously decrease the volume ratio of casting porosity from 2.29% to 0.21%. Additionally, the γ' phase in both the dendritic and inter-dendritic regions undergoes refinement, with a more uniform size distribution and a more regular shape. After the subsequent solid solution and aging treatments, the smaller γ' precipitates with higher cubic degree are obtained in samples after dendrite refinement, whose service life at 980 °C/280 MPa is improved by 13.8%.

Key words: nickel-based single-crystal superalloy; dendrite refinement; microstructure; eutectic; γ' phase; stress rupture properties

1 Introduction

Superalloys are widely employed in industrial applications owing to their outstanding thermal performance[1–6]. Nickel-based single-crystal superalloys have been widely used to produce high-pressure turbine blade and vanes of aero engine by directional solidification technique[3,7]. Dendrite is typically formed, and the primary dendrite spacing (λ_1) is a critical microstructural parameter for controlling final microstructure and properties. Previous researches showed that higher λ_1 corresponds to a higher fraction of pores and coarser precipitates (such as γ/γ' eutectic and *M*C carbides), as well as increased difficulty to homogenize elemental segregation between dendrites during subsequent solid-solution treatment[8–10]. Noteworthy, temperature gradient G is the key parameter affecting λ_1. The maximum G is often in the range of 2–3 K/mm primarily due to the ineffective thermal-insulation between heating zone and cooling zone of the directional solidification furnace, leading to λ_1 within the range of 0.4–0.5 mm or even higher, and thereby affecting the mechanical properties of the Ni-based single-crystal superalloys. Meanwhile, the coarsening of primary dendrite spacing can lead to an increase in diffusion distance of alloying elements during heat treatment, further increasing the difficulty of element homogenization. In the past decades, dendrite refinement primarily relies on the change of solidification parameters, such as increasing withdrawing rate or changing cooling method (liquid metal cooling), whereas other technical issues emerge, such as the fluctuation of cooling rate that is related to the formation of dendrites and eutectics[11–15].

Furthermore, for nouveau-generation single-crystal superalloy, as the percentage of refractory elements (W+Re+Mo) increases[16–18], elemental segregation between dendrite and

Received date: June 20, 2025
Foundation item: Shenzhen Science and Technology Program (JSGG20220831092800001)
Corresponding author: Huang Zaiwang, Ph. D., Professor, State Key Laboratory of Powder Metallurgy, Central South University, Changsha 410083, P. R. China, E-mail: huangzaiwang@csu.edu.cn

inter-dendritic regions becomes more severe, in accompany with a higher fraction of eutectics in inter-dendritic region and incomplete dissolution during heat treatment. Thus, decreasing primary dendrite spacing becomes highly desirable to address the abovementioned technical problems.

In this research, a conformal thermal-insulation unit that can realize a temperature gradient as high as 4 – 5 K/mm between heating zone and cooling zone was designed, while other solidification parameters, such as pouring temperature and withdrawing rate, kept unchanged. The improvement of temperature gradient provided a unique pathway to refine primary dendrite spacing, and its effect on the microstructure and mechanical properties was investigated, providing an opportunity to explore potential engineering applications.

2 Experiment

The nominal composition of the new third-generation single-crystal superalloy WZ30 is shown in Table 1. The master alloy was prepared using vacuum induction melting furnace (Consarc VIM-50). The single-crystal rod with a diameter of 15 mm and a length of 170 mm was cast using conventional method in directional solidification furnace (ALD, Germany). And a novel technique that can control temperature gradient up to 4 – 5 K/mm was also applied to prepare single-crystal rod, whose dendrite was refined. The processing parameters for both conventional and novel techniques were as follows: mold holding temperature of 1550 ° C, pouring temperature of 1520 ° C, and mold withdrawal rate of 3 mm/min.

Table 1 Nominal composition of the new third-generation Ni-based superalloy WZ30 (wt%)

Cr	Co	W	Mo	Al	Ti	Ta	Re	Nb	Ni
3.50	6.00	6.50	0.40	5.80	0.15	8.00	4.95	0.10	Bal.

The heat treatment process for WZ30 superalloy was 1280 °C/9 h+1310 °C/7.5 h+1325 °C/9.5 h+1340 °C/6 h/air cooling (AC) +1140 ° C/6 h/AC+870 ° C/16 h/AC using a vacuum furnace (15.0VPT-4022/24HVIQ, SECO/WARWICK). The samples were ground, polished, and etched using standard processes. The center position of the rod was observed for comparing the microstructures of as-cast and heat-treated samples using optical microscope (OM, NIKON MM-400) and scanning electron microscope (SEM, FEI Quanta 650 FEG). Rupture tests were performed at 980 °C/280 MPa according to ASTM standard. Transmission electron microscope (TEM) operating at 200 kV was used to observe the microstructures of the fracture of ruptured samples.

3 Results and Discussion

The dendritic microstructures of both conventional and dendrite-refined samples are presented in Fig. 1a and 1b, respectively. For the conventional alloy, the average primary dendrite spacing is about 415 μm, and the secondary dendrite arms are coarsened due to lower temperature gradient. Numerous tertiary dendrite arms can even be observed (Fig. 1a). The dendrites of refined alloys are more uniformly distributed (Fig. 1b), and average primary dendrite spacing is measured to be 251 μm. The secondary dendrite arms become finer, while tertiary dendrites disappear. Moreover, the alloy with coarser dendrite structure has a higher fraction of eutectics (around 12%) than that with finer dendrite structure (9%), and its average size is relatively higher.

Fig. 2 shows pores (black holes) formed during directional solidification. It is evident that the average size of pores of

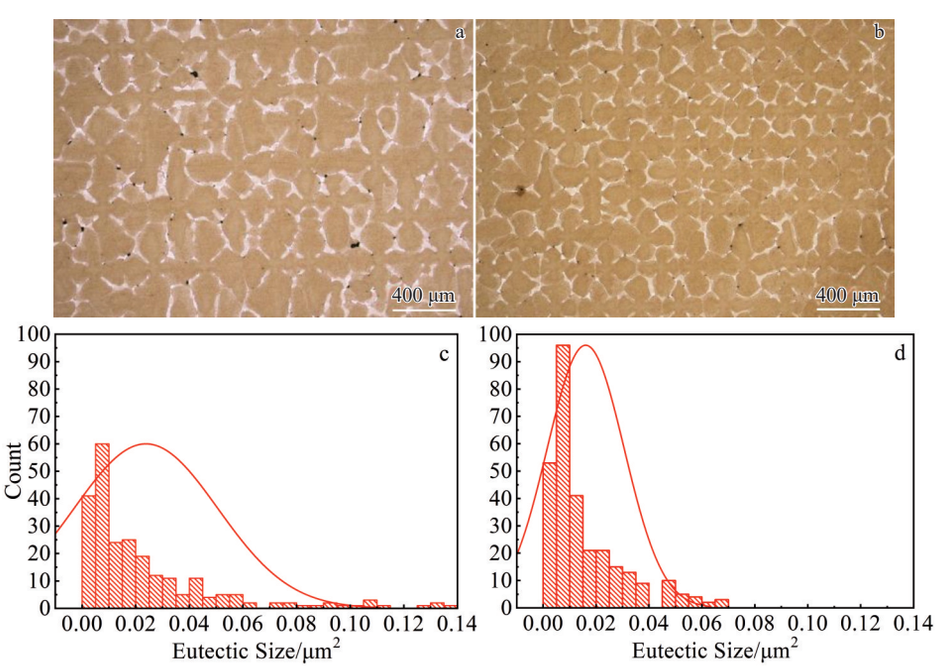

Fig.1 OM images (a–b) and eutectic size distributions (c–d) of as-cast WZ30 single-crystal superalloys: (a, c) conventional sample; (b, d) dendrite-refined sample

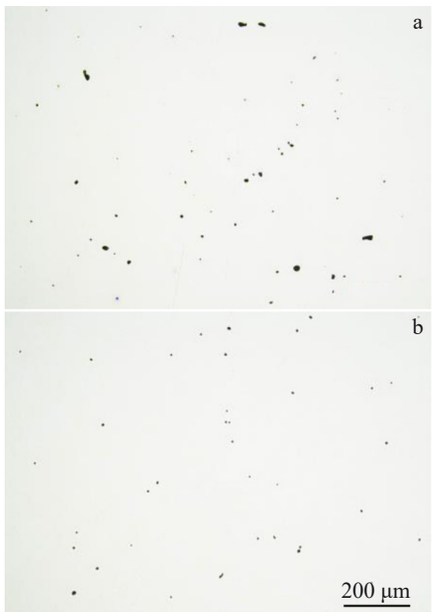

Fig.2 Microstructures of pores of as-cast WZ30 single-crystal superalloys: (a) conventional sample; (b) dendrite-refined sample

conventional sample is larger (Fig. 2a), and its porosity is measured up to 2.29%. In contrast, the average size of pores of dendrite-refined sample is obviously smaller (Fig. 2b), and the porosity decreases to 0.21%. Thus, the dendrite refinement can simultaneously decrease the casting porosity.

Fig. 3 shows the γ' phase morphologies and size distribution of both conventional and dendrite-refined samples. In general, the average size of γ' phases in the dendrite core is smaller than that in the interdendritic region for both samples (Fig. 3a–3d). The average size of γ' phases of conventional sample is relatively smaller compared to that of dendrite-refined sample in both dendrite core and interdendrite region (Fig. 3c – 3d), which is attributed to the higher temperature gradient.

After solid solution and aging heat treatment, it can be seen that the γ' phase in both samples shows obvious coarsening and tends to form cubic structures, particularly in dendrite core. In comparison, the γ' phases in the interdendritic region exhibit less morphological regularity. After heat treatment, the volume fraction of γ' phase of conventional and dendrite-refined samples is 58.75% and 59.81%, respectively. From Fig. 4a and 4c, the size and morphology of γ' phase in the dendrite core of both samples are almost the same, whereas the average size of the γ' phase in the interdendritic regions of conventional sample is slightly larger compared to that in the dendrite core, and its morphology is relatively irregular (Fig. 4d). This manifestation is closely related to the higher eutectic content in the as-cast conventional alloys, since the eutectic structure is not fully dissolved after solid solution heat treatment.

Table 2 presents the stress rupture properties (average rupture time) of heat-treated WZ30 single-crystal superalloys tested at 980 °C/280 MPa. By contrast, the stress rupture properties of the dendrite-refined sample is remarkably improved, and the average rupture time increases from 217 h to 247 h, leading to a 13.8% improvement in rupture life.

Fig. 5 presents fracture surface morphologies of conventional and dendrite-refined samples. The necking occurs in both samples after stress rupture tests, and the fracture surface is basically normal to the loading direction. Fig. 5b and 5d show the dimples and pores, which are closely associated with the initiation of cracking. Owing to the absence of grain

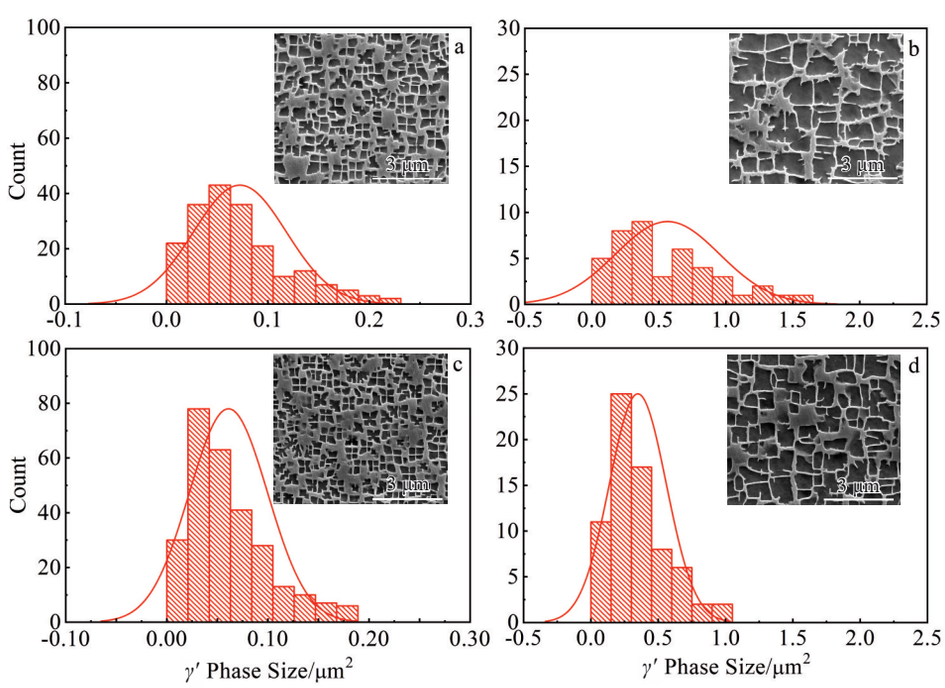

Fig.3 Size distribution histograms coupled with SEM images of γ' phase in the dendrite core (a, c) and interdendrite region (b, d) of as-cast WZ30 single-crystal superalloys: (a–b) conventional sample; (c–d) dendrite-refined sample

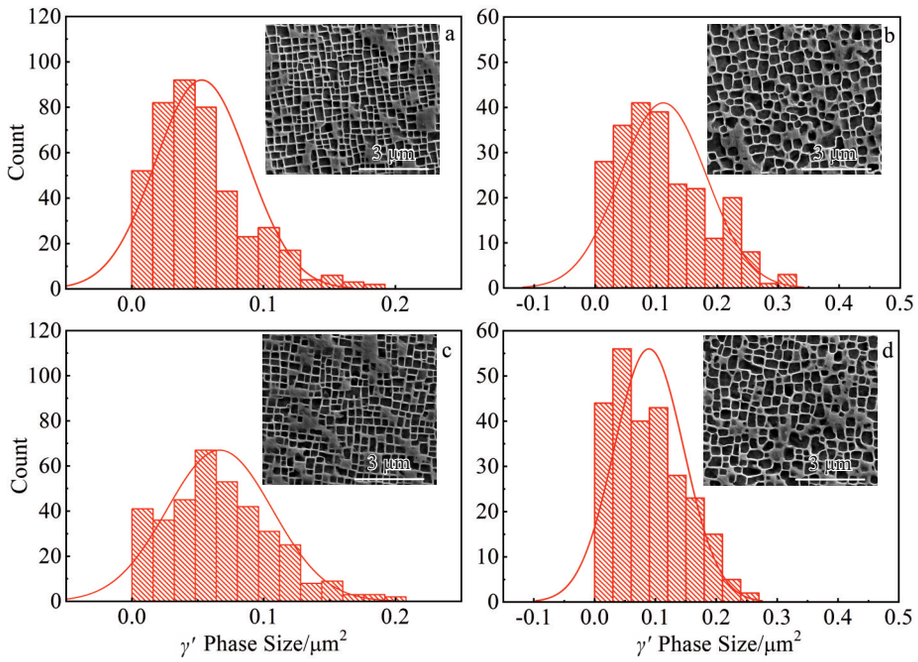

Fig.4 Size distribution histograms coupled with SEM images of γ' phase in the dendrite core (a, c) and interdendrite region (b, d) of heat-treated WZ30 single-crystal superalloys: (a–b) conventional sample; (c–d) dendrite-refined sample

Table 2 Properties of heat-treated WZ30 single-crystal superalloys

Sample	Average primary dendrite spacing/μm	Porosity/%	Eutectic fraction/%	Volume fraction of γ' phase/%	Average rupture time/h
Conventional	415	2.29	12	58.75	217
Dendrite-refined	251	0.21	9	59.81	247

boundary, the rupture failure of the single-crystal superalloy is largely controlled by the initiation and growth of pores. Based on Fig. 5b and 5d, the pores are found in the middle part of cleavage zone and propagate along <001> direction, resulting in the formation of smooth square-shaped cleavage plane (white dotted line)[19–22]. However, the number of pores on the fracture plane of dendrite-refined sample (Fig.5d) is obviously less than that of conventional sample (Fig.5b). Thus, it can be concluded that the refinement of dendritic structure can significantly inhibit the formation of pores and improve the stress rupture properties.

Fig.6 shows the deformed microstructures of γ matrix and γ' precipitates observed on both cross and longitudinal sections of WZ30 samples after stress rupture testing at 980 ° C/ 280 MPa, and the sample was cut 5 mm away from the fracture surface. On the cross section, the cuboid-shaped γ' phases (dark region) after stress rupture testing are fully transformed to irregular structures, but their volume fractions are 53.98% and 53.05% in the conventional (Fig. 6a) and dendrite-refined (Fig. 6b) samples, respectively, which are slightly less than those of the heat-treated samples (58.75% and 59.81%). The coarsening and coalescence of γ' phases can be observed, and interlayer of γ channels is absent. On the longitudinal section, the γ' precipitates exhibit pronounced raft-like morphology, with the elongated orientation perpendicular to the applied stress direction. In comparison, the morphology of deformed γ' phase of conventional sample is more irregular than that of dendrite-refined sample, indicating that the stress rupture property is dependent on the evolution of the γ' phase morphology.

Fig. 7 shows low-magnification pore morphologies on longitudinal section near the fracture surfaces of samples after stress rupture fracture. It can be seen that pores can be observed in both samples, and the closer the distance to the fracture plane, the higher the porosity. This phenomenon primarily results from pore formation in final-solidifying inter-dendritic regions due to inadequate liquid-alloy feeding during solidification. These pores are typically spherical or irregular in shape and are classified to casting pores. Upon stress rupture test, the growth of pores can lead to the coalescence and premature fracture. Based on the observations, the dendrite-refined sample (Fig. 7b) has a remarkably lower number of pores compared to the conventional sample (Fig. 7a), which demonstrates that dendrite-refined samples has less pores in interdendritic region after stress rupture test, resulting in improved rupture properties.

To further compare their difference, Fig. 8 illustrates the dependence of the number and size of pores and microcracks

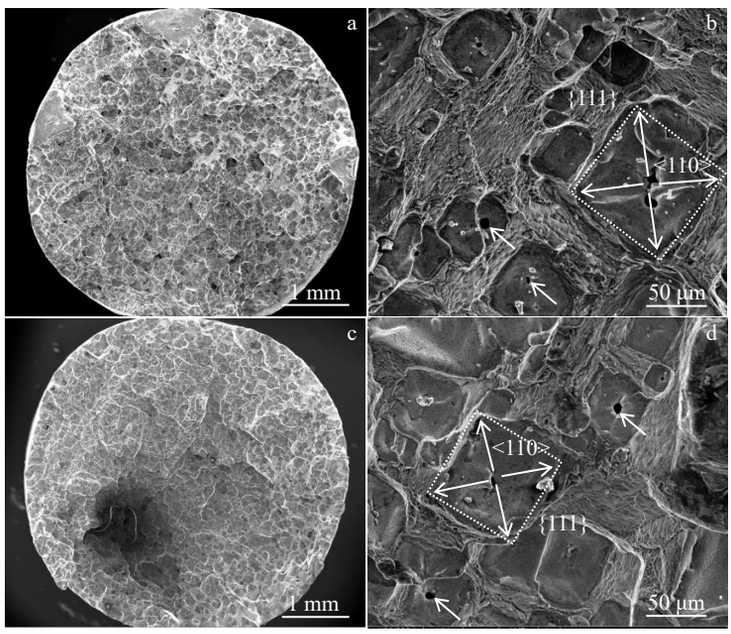

Fig.5 Fracture morphologies of conventional (a–b) and dendrite-refined (c–d) samples

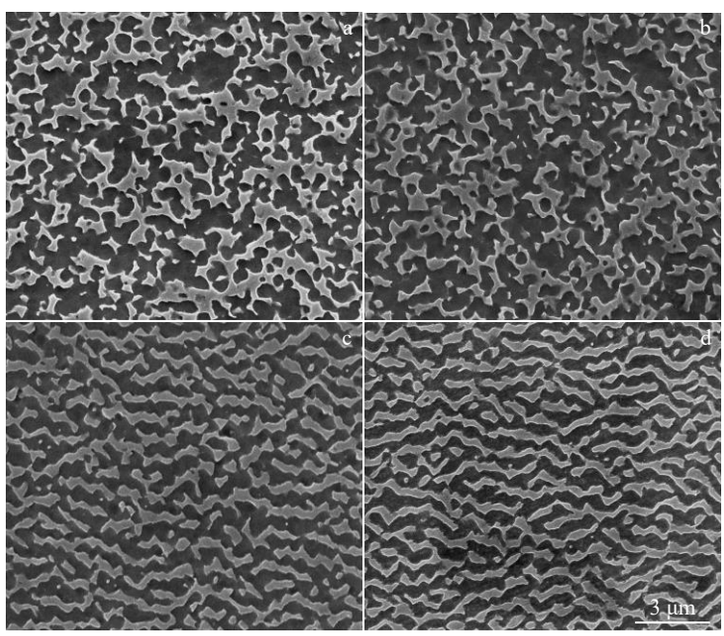

Fig.6 γ′ phase morphologies on cross (a–b) and longitudinal sections (c–d) of heat-treated WZ30 single-crystal superalloy after rupture test at 980 °C/280 MPa : (a, c) conventional sample; (b, d) dendrite-refined sample

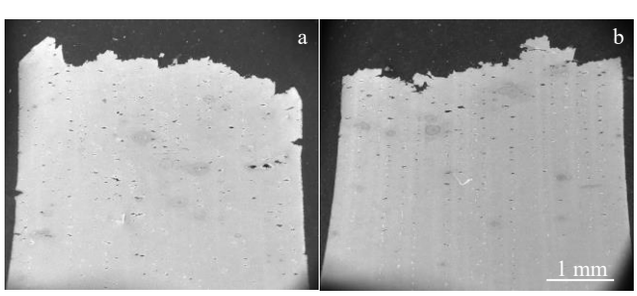

Fig.7 Low-magnification pore morphologies on longitudinal section of ruptured samples tested at 980 °C/280 MPa: (a) conventional sample; (b) dendrite-refined sample

on the regions away from fracture surface in conventional and dendrite-refined samples ruptured at 980 °C/280 MPa. For the dendrite-refined sample, the number and size of pores are obviously increased when the distance is short, but they are still smaller compared to those of conventional sample. Under both conditions, the pores exhibit an elliptical morphology, with their major axes oriented perpendicular to the applied stress direction. It is evident that the non-uniform pores are present in interdendritic region of as-cast alloy. After heat treatment, due to the diffusion and homogenization of elements, some spherical pores form. Epishin et al[23] found that interior vacancies can migrate towards the surface under

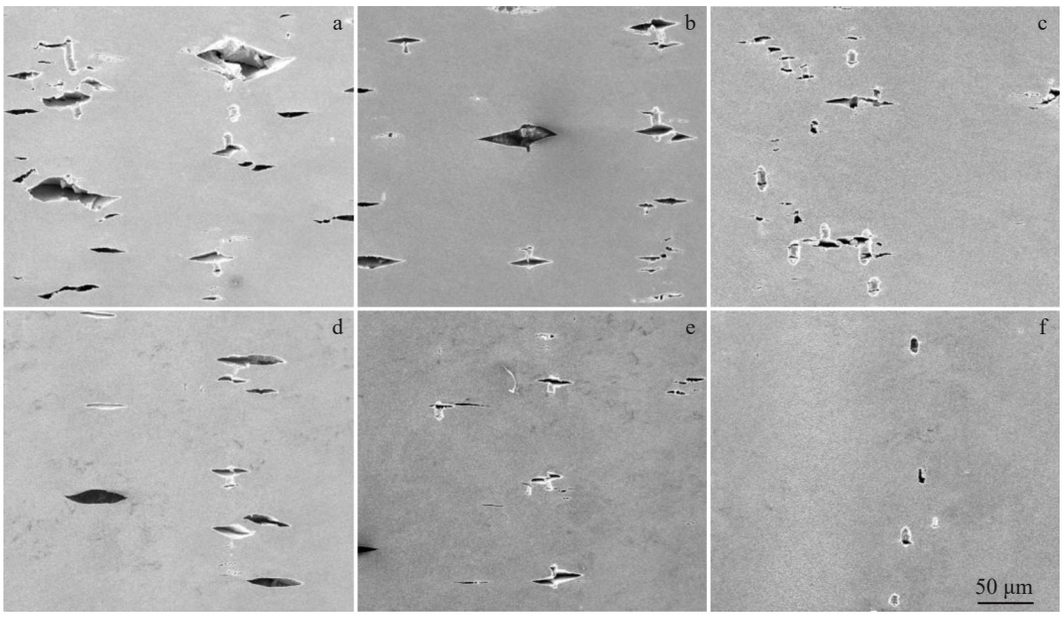

Fig.8 Pore morphologies on the longitudinal section of the conventional (a–c) and dendrite-refined (d–f) samples at different distances from the fracture surface: (a, d) 1 mm; (b, e) 5 mm; (c, f) 9 mm

the influence of temperature and stress. When interior vacancies encounter with pores, the growth of pores can be accelerated. It is noteworthy that vacancies prefer to locate on the {111} planes in the vicinity of pores, leading to lateral growth nearby {001} planes. This behavior can result in the formation of hexahedron, octahedron, and dodecahedron around the pores[24]. Under the influence of temperature and stress, rectangular pores undergo elongation along the stress direction, resulting in a higher cubic degree. Subsequently, as the creep deformation continues, the elliptical distortion is initiated at both ends of the pore, eventually evolving into elongated pores (perpendicular to stress direction) and micro-cracks. The continuous growth and coalescence of microcracks eventually lead to the fracture.

Fig. 9 shows TEM images of deformed microstructures (5 mm away from fracture plane) of conventional and dendrite-refined samples. Bright-field TEM images show that the dislocations of high density exist within the γ channel. These dislocation networks exhibit irregular shapes, which are predominantly quadrilateral and hexagonal. Simultaneously, it is evident that the irregular γ' phase contains a higher concentration of super-dislocations, consisting of two parallel pairs of dislocations[25]. Most of the super-dislocations are located within the γ' phase, although it has been observed that some of them are also associated with the dislocation network in the γ matrix. When comparing Fig. 9a and 9b, it can be found that dendrite refinement can reduce dislocation network spacing within the γ matrix, resulting in a finer network. Additionally, the majority of the dislocation network exhibits a square shape with more regularity. The refined dislocation network significantly hinders the movement of dislocations, resulting in a lower density of super-dislocations during the cutting of γ' phase[25–26].

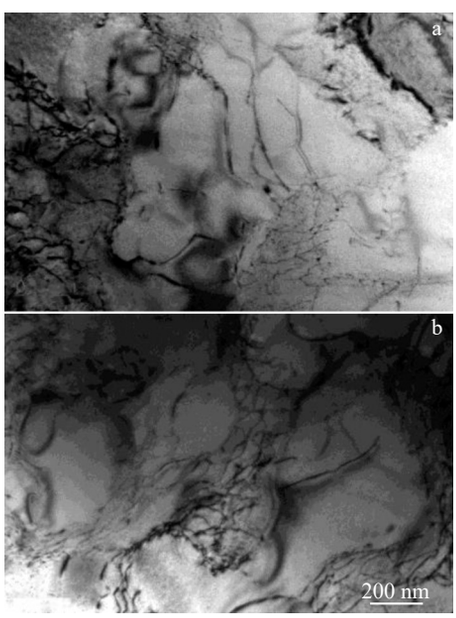

Fig.9 TEM images of cross section of the conventional (a) and dendrite-refined (b) samples at 5 mm away from the fracture surface

4 Conclusions

1) Compared to those of the conventional sample of WZ30 Ni-based single crystal superalloys, the average size, volume fraction of eutectics, and casting porosity of dendrite-refined sample are relatively smaller. Moreover, the average size of γ' phases of dendrite-refined sample at as-cast state is larger in both dendrite core and inter-dendrite region.

2) The casting porosity of dendrite-refined sample is significantly reduced, leading to a 13.8% improvement in

rupture life at 980 °C/280 MPa.

3) After stress rupture fracture, the γ′ phases of dendrite-refined sample near the fracture surface exhibit obvious raft-like morphology with higher cubic degree. The spacing of dislocation networks of dendrite-refined sample is reduced, resulting in a finer and more regular dislocation network, as well as the super-dislocations of low density in the γ′ phase.

References

1 Pan Y, Jin C. *Vacuum*[J], 2017, 143: 165
2 Pan Y, Wen M. *Vacuum*[J], 2018, 156: 419
3 Reed R C. *Superalloys: Fundamentals and Applications*[M], Cambridge: Cambridge University Press, 2006
4 Pan Y, Pu D L, Li Y Q *et al*. *Materials Science and Engineering B*[J], 2020, 259: 114580
5 Pan Y, Pu D L. *Ceramics International*[J], 2020, 45(5): 6698
6 Pan Y, Chen X W, Zhang X Y. *Vacuum*[J], 2023, 212: 112033
7 Caron P, Khan T. *Aerospace Science and Technology*[J], 1999, 3(8): 513
8 Zhang Xiaoyue, Liu Lin, Huang Taiwen *et al. Rare Metal Materials and Engineering*[J], 2013, 42(12): 2547 (in Chinese)
9 Yu Z H, Liu L, Zhao X B *et al. China Foundry*[J], 2010, 7(3): 217
10 Jin Tao, Li Jinguo, Zhao Nairen *et al. Journal of Materials Engineering*[J], 2002, 30(3): 36 (in Chinese)
11 Wang F, Ma D X, Bogner S *et al. Metallurgical and Materials Transactions A*[J], 2016, 47(7): 3703
12 Zhang J, Lou L H. *Journal of Materials Science & Technology*[J], 2007, 23(3): 289
13 Fu H Z, Geng X G. *Science and Technology of Advanced Materials*[J], 2001, 2(1): 197
14 Yang Y Z, Wen Z X, Pei H Q *et al. Progress in Natural Science: Materials International*[J], 2023, 33(3): 343
15 Xu F Z, Xiong W, Lin Y C *et al. Journal of Materials Research and Technology*[J], 2024, 33: 8252
16 Sato A, Harada H, Yeh A C *et al. Superalloys 2008*[C]. Champion: TMS, 2008: 131
17 Ma Dexin, Zhao Yunxin, Li Qingtao *et al. Rare Metal Materials and Engineering*[J], 2021, 50(9): 3320 (in Chinese)
18 Zhang Longfei, Jiang Liang, Zhou Kechao *et al. The Chinese Journal of Nonferrous Metals*[J], 2022, 32(3): 630 (in Chinese)
19 Wen Z X, Zhang D X, Li S W *et al. Journal of Alloys and Compounds*[J], 2017, 692: 301
20 Tian S G, Ding X, Guo Z G *et al. Materials Science and Engineering A*[J], 2014, 594: 7
21 Wang G L, Qi D Q, Liu J L *et al. Journal of Materials Science & Technology*[J], 2023, 163: 237
22 Wang G L, Liu J L, Liu J D *et al. Journal of Materials Science & Technology*[J], 2016, 32(10): 1003
23 Epishin A, Link T. *Philosophical Magazine*[J], 2004, 84(19): 1979
24 Yue Quanzhao. *Elevated Temperature Creep Behavior and Mechanism of the Third-Generation Ni-Based Single Crystal Superalloy DD33*[D]. Xi'an: Northwestern Polytechnical University, 2019 (in Chinese)
25 Wang X G, Liu J L, Jin T. *Materials Science and Engineering A*[J], 2015, 626: 406
26 Zhang J X, Murakumo T, Koizumi Y *et al. Acta Materialia*[J], 2003, 51(17): 5073

枝晶细化对第三代镍基单晶高温合金显微组织和持久性能的影响

赵运兴[2,3]，王　迪[1,2]，马德新[2,3]，魏剑辉[2,3]，程博文[3]，孙洪元[2,3]，徐维台[3]，黄再旺[1,2]

(1. 中南大学 粉末冶金国家重点实验室，湖南 长沙 410083)

(2. 中南大学 粉末冶金研究院，湖南 长沙 410083)

(3. 深圳市万泽航空科技有限责任公司，广东 深圳 518045)

摘　要：采用第三代单晶高温合金WZ30，在不同工艺条件下制备了具有不同枝晶间距的单晶试样，并对其显微组织和持久性能进行了研究和比较。结果表明，通过改进定向凝固炉加热室与冷却区之间的隔热效果，试样铸件的平均一次枝晶间距从415 μm减小至251 μm，实现了枝晶和共晶组织的显著细化。同时，枝晶细化后，样品中铸造孔隙率比从2.29%降低至0.21%。此外，枝晶细化后，样品中枝晶干和枝晶间区域的γ′相均发生细化，尺寸分布更加均匀，形状更加规则。经过后续固溶和时效处理后，枝晶细化试样获得了尺寸更小、立方度更高的γ′析出相。在980 ℃/280 MPa条件下，枝晶细化后样品的持久寿命提高了13.8%。

关键词：镍基单晶高温合金；枝晶细化；显微组织；共晶；γ′相；持久性能

作者简介：赵运兴，男，1988年生，博士，工程师，中南大学粉末冶金研究院，湖南 长沙 410083，E-mail：zhaoyunxing@csu.edu.cn